Biosensors and Bioelectronics 101 (2018) 96–102

Contents lists available at ScienceDirect

Biosensors and Bioelectronics

journal homepage: www.elsevier.com/locate/bios

A shape-code nanoplasmonic biosensor for multiplex detection of Alzheimer's disease biomarkers

Hanbi Kim, Jong Uk Lee, Sojin Song, Soohyun Kim, Sang Jun Sim*

Department of Chemical and Biological Engineering, Korea University, Seoul 02841, South Korea

ARTICLE INFO

Keywords:
Shape-code
Multiplex detection
Alzheimer's disease (AD)
Gold nanoparticles (AuNPs)
Plasmonic biosensors
Localized surface plasmon resonance (LSPR)

ABSTRACT

Alzheimer's disease (AD) is a neurodegenerative disease associated with the loss of nerve cells in the brain. The disease is affected by multifactorial pathways and leads to changes in related biomolecular levels as AD progresses. Therefore, AD should be diagnosed with combined detection of several lesions to improve accuracy. Amyloid beta 1–40, 1–42 and τ (tau) protein are milestones in AD pathology and can be used as main screening and diagnostic target markers. Here, we suggest a highly selective biosensor for detection of AD core biomarkers on one platform through distinct localized surface plasmon resonance (LSPR) depending on gold nanoparticles shapes, called a shape-code biosensor. This plasmonic sensor consists of only gold nanoparticles and antibody, but does not need additory methods for precise separation from multifarious samples and identification of markers. Under physiological condition, we determined a detection limit of 34.9 fM for amyloid beta (Aβ) 1–40, 26 fM for Aβ 1–42 and 23.6 fM for τ protein corresponding to the ~ 1, ~ 2.23 and ~ 3.12 nm of Rayleigh scattering peak shift on shape-code plasmon system for each biomarker in mimicked blood. This is the first highly sensitive shape-code biosensor to detect AD biomarkers which can be used to diagnose AD easily in the future.

1. Introduction

Alzheimer's disease (AD) is an irreversible neurodegenerative disease causing severe cognitive decline and is the most frequent form of dementia in the elderly (Liu et al., 2013).

The disease is generated by complex pathological ways and several molecules, such as formation of amyloid load, tauopathy, inflammation and oxidation damage (Gupta et al., 2013). The formation of amyloid senile plaques and neurofibrillary tangles in the brain is a hallmark of AD (Citron et al., 1995). Amyloid plaques mainly contain overexpressed amyloid beta (Aβ) 1–40 and Aβ 1–42 derived from the abnormal processing of amyloid precursor protein (APP) (Citron et al., 1995). Extracellular deposits of proteins and resulting plaques generate neurotoxicity in the brain by interrupting signal transfers between neurons (Kanekiyo et al., 2014; Liao et al., 2012). There is growing evidence that simultaneous or perhaps even earlier neurofibrillary tangles are composed of intraneuronal aggregates of abnormally hyper-phosphorylated τ proteins disengaged from microtubules (Frank et al., 2003; Martin et al., 2011). Dissociation of τ protein leads to collapse of microtubules and impairs the neuron system (Martin et al., 2011).

Some pathological processes are similar with senility in the aged, for example, the concentration of both amyloid beta (Aβ) 1–40 and Aβ 1–42 increases with age older than 65 and increments are also known as a beginning milestone of amyloid aggregation in the brain of AD patients. Yet, as the lesion progresses, plasma Aβ 1–42 level diminishes at an average rate of 12% per year in people with AD and concentration of plasma Aβ 1–40 rises constantly regardless of having the disease (Van Oijen et al., 2006). In addition, a growing body of literature has revealed that Aβ amyloid deposition in the brain correlates inversely with concentration of Aβ 1–42, while τ protein levels reflect the stage of neuronal degeneration and brain damage (Kang et al., 2012). Consequently, Aβ1–40, Aβ1–42 and τ protein, the constituents of the amyloid load and neurofibrillary tangles, respectively, are considered as reliable and complementary biomarkers for AD diagnosis based on combined detection (Frank et al., 2003; Schneider et al., 2009). AD patients cannot be accurately diagnosed by individual physiological variation due to the heterogeneity of dementia pathology. It is imperative to deviate from the traditional approach of investigation standardized on single biomarker candidates and develop diagnosis methodology of multiplex biomarker detection to reflect the complexity of AD pathogenesis. Simultaneous detection of two or more markers achieves higher sensitivity than one marker to distinguish Alzheimer's disease patients and others, indicating that each marker may be complementary and not redundant with the other for accurate diagnosis (Abdi et al.,

* Corresponding author.
E-mail address: simsj@korea.ac.kr (S.J. Sim).

http://dx.doi.org/10.1016/j.bios.2017.10.018
Received 8 September 2017; Accepted 9 October 2017
Available online 11 October 2017
0956-5663/

2006). For instance, the combination of AD core biomarkers (e.g. Aβ and τ protein) revealed balanced value of prediction factor for distinguishing of AD from healthy control as 85.7% of sensitivity and 84.6% of specificity with ratio τ protein/Aβ1–42 in brain, as compared with single biomarker based methodology (tau with 69.6% and 92.3% of sensitivity and specificity; Aβ1–42 with 96.4% and 76.9% of sensitivity and specificity, respectively) (Shaw et al., 2009).

To this end, many studies have formulated groundbreaking methods to discriminate between age-matched controls and AD patients and evaluated different combinations of protein chips to yield high sensitivity and specificity (Hye et al., 2006), but thus far, existing methods are predominantly required two steps that are same as cognate with conventional protein identification and measurement: separation of proteins biomarkers from sample and peptide ionization for quantification of targeted markers. The first separation process is accomplished by two-dimensional polyacrylamide gel electrophoresis (2D-PAGE) or high-performance liquid chromatography (HPLC) (Butterfield et al., 2003); surface chromatography absorbing proteins to activated surfaces (Carrette et al., 2003) and then mass spectroscopy (MS) is used for peptide ionization procedures from gels or protein chips as quantitative measurement of the target molecules. While these technologies are typically accessible to researchers, they are incapable of application for low molecular weighted, hydrophobic peptides and heterogeneous compounds as well as measurement of dynamic quantitative range. Surface enhanced laser desorption/ionization-time of flight MS has been newly introduced with more thorough quantification and capture of native proteins, notwithstanding complex procedure is required for post-processing and reproduction (Gupta et al., 2013). Other universal studies have been based on enzyme-linked immunosorbent assay (ELISA) methodology such as xMAP-Luminex multiplex platform using Innogenetics AlzBio3 immunoassay reagents to detect concentration of Aβ 1–42, total τ protein and phosphorylated τ protein at 181 (Kang et al., 2012). It improved dynamic range and decreased required sample volume to approximately half for analyses of three biomarkers as compared to conventional ELISA, but requires 10 handling steps and 19 h to analyze three biomarkers, totally.

In this study, we suggest a highly selective non-labeling platform for analyzing three predominant AD biomarkers including Aβ 1–40, Aβ 1–42 and τ protein using an ultra-sensitive 'shape-code' nanoplasmonic sensor. We simultaneously exploit three different kinds of immuno-AuNPs, such as spheres (diameter of 50 nm), short rods (aspect ratio of 1.6) and long rods (aspect ratio of 3.6) for detecting Aβ 1–40, Aβ 1–42 and τ protein, respectively, showing individual properties on optical spectrometers as if the bar-code is scanned. Nanoparticles consisted of 'shape-code' plasmonic biosensor based on localized surface plasmon resonance (LSPR). The plasmonic biosensor under the electromagnetic field of incoming light enables detection of incident photon frequency produced by collective coherent oscillation of free electrons that hem in nanometer-sized metallic particles. The result is Rayleigh light scattering, called LSPR (McFarland and Duyne, 2003; Anker et al., 2008; Lee et al., 2015). The plasmon resonance wavelength on the surface of the nanoparticle (LSPR) is dependent on shape, size, and local refractive index surrounding AuNPs (Lee et al., 2015). On this account, varied shapes and sizes easily tune optical properties of gold nanoparticles including surface plasmon resonance wavelength without any dyes (Link et al., 2000). Since the λ_{max} position directly relates to the color of AuNPs in dark-field, recognition of each immuno-particle can easily be conducted without labeling steps or scattering measurements (Gish et al., 2007; Rosi and Mirkin, 2005; Truong et al., 2012). Also, this nanoplasmonic biosensor sensitively detects molecular interaction (e.g. antibody-protein interactions and DNA hybridization) occurring on the surface of gold nanoparticles, since surface-bound events arise from changes in the dielectric environment surrounding the particle having significant effect on the extinction peak (λ_{max}) of nanomaterials (Hall et al., 2011). Based on that, our 'shape-code' plasmonic biosensor detects individual antibody-protein interaction on distinct immuno-gold nanoparticles (AuNPs) and the colorimetric feature of it enables multiplex detection of biomarkers from single sample without additional steps for protein identification. It also reduces analytical time via detection of three biomarkers in one analytical run and increases detected throughput. Such highly sensitive and selective immunoassays in multiplexed fashion are essential methods for disease diagnostics, therapeutics and biodefense applications (Stoeva et al., 2006). As a consequence, we successfully developed a novel methodology for detecting AD-related biomarkers with considerably high selectivity, sensitivity and close approach to AD complex pathway promoting realization of diagnosis of AD.

2. Materials and methods

2.1. Materials

NHydroxysuccinimide (NHS), sodium citrate, absolute ethanol, 3-aminopropyltriethoxysilane (APTES), sodium citrate, L-ascorbic acid, silver nitrate ($AgNO_3$, > 99%), NethylN(diethylaminopropyl)carbodiimide (EDC), sodium borohydride, gold(III) chloride trihydrate (≥ 99.0%), dimethyl sulfoxide (DMSO), Sodium borohydride ($NaBH_4$, 99%), hydrochloric acid (HCl, 37 wt% in water), Hexadecyltrimethylammonium bromide (CTAB, > 98.0%) were purchased from Sigma Aldrich (Korea). Sodium oleate (NaOL, > 97.0%) was purchased from TCI America. COOH-PEG-SH (Mw 2000, 3400 and 5000) was purchased from Laysan Bio, Inc. Anti-Aβ 1–40 antibody and recombinant Aβ 1–42 were purchased from Abcam. Anti- Aβ 1–42 antibody was purchased from Millipore. Recombinant Aβ 1–40 was purchased from Anaspec. Coverslip slides (22 × 40 × 0.1 mm) were purchased from Deckglaser (Germany). Ultra–pure water (18.2 mΩ cm^{-1}) was used to prepare all solutions.

2.2. Preparation of gold nanoparticles for shape-code biosensor

Gold nanoparticles (AuNPs) were synthesized citrate reduction method for gold nanospheres and seed-mediated growth method of gold nanorods followed synthesized methods in previous studies (Jv et al., 2010; Ye et al., 2013). To connect with antibody and render gold nanoparticle stable in physiological conditions, heterofunctionalized polyethylene glycol (PEG) was used as a ligand to functionalize the surface on gold nanoparticles.

For functionalization of 50 nm gold nanospheres, 20 μL of 1 mM PEG (Mw 2000) was added in 1 mL of synthesized AuNSs solution and mixed with full turn for 24 h. The mixture was centrifuged at 7000 rpm for 15 min to discard excess PEG molecules and unreactive AuNPs, and re-suspend in 100 μL of deionized water. Conversely, gold nanorods were functionalized with longer polyethylene glycol. 40 mg of Mw 3400 or 5000 PEG were proportionally mixed to 2 mL AuNRs solution (300 μg Au/mL). Resulting solution was centrifuged at 5000 rpm for four minutes after which the mixture was swirled vigorously for four days.

On subsequent step to conjugate antibody to carboxylated gold nanoparticles, 3 μL of 0.7 M EDC/NHS was mixed with 300 μL of functionalized gold nanoparticles solution to convert carboxyl groups of PEG to NHS esters for connecting with amine group of antibodies after 15 min, 150 μL of each target protein monoclonal antibody (mAb) (50 μg/mL) was added to ester activated AuNPs solution. The solutions were mixed overall and incubated at room temperature. After four hours, the immune-gold nanoparticles were centrifuged at 5000 rpm for 10 min or 3000 rpm for four minutes to separate unreactive particles and molecules. The pellet was re-dispersed in deionized water and stored at 4 °C for stabilization.

2.3. Fabrication of multiplex detection platform based on shape-code AuNPs

For nanoplasmonic biosensor fabrication, immuno-gold nanoparticles were diluted to optical density (OD) 0.05 at peak wavelength and mixed with the same volume of diluted solution in a tube. The 10 μL of immuno-gold nanoparticles solution was incubated for two minutes to drop-coat onto 10% (v/v) APTES-coated glass. The glass slide was mounted to a closed bath imaging chamber to visualize AuNPs after addition of reactants. The chamber was subsequently inserted onto the holder of the dark–field microscope, and fluidic flow was set at 100 μL/min with connection to a syringe pump (Anker et al., 2008). LSPR shift measured particles were chose by colored spot in dark-field microscope and the changes of λ_{max} wavelength are recorded after every chemical step. Initially, the surface of the glass slide was washed through DI for 30 min to expunge contaminants and unbound immune gold nanoparticles. Then, 1 mL of ethanolamine (0.2 M) solution was injected into the chamber and incubated for 30 min to inhibit non-specific binding on unreactive surface of AuNPs. Subsequently, varied concentrations of three Alzheimer's disease biomarkers ranging from $1 * 10^1$ fM to $1 * 10^8$ fM, were diluted in Dulbecco's phosphate buffered saline (D-PBS, pH 6.95) and mixed in human plasma samples (pH 7.82) that are remained into pH of biologic solution. Those antigen-plasma complexes were flowed onto the surface of immune-AuNPs and incubated for one hour. Nanoplasmonic biosensors on the glass slide were cleaned through ultra-pure water into flow cell for five minutes after each reactive step, and distinct Rayleigh light scattering occurred on the sensor after analyte binding was measured through dark-field, a spectrograph, and CCD camera (Fig. 1). To determine plasmon shift ($\Delta\lambda_{max}$) of the LSPR spectra occurring on the sensor, the wavelength shift $\Delta\lambda_{max}$ was analyzed with the following formula: λ_{max} (after reaction) – λ_{max} (before reaction) after fitting with the Lorentzian algorithm using OriginPro 8 software and GraphPad Prism 5 software.

2.4. X-ray photoelectron spectroscopy (XPS)

XPS was used to confirm successful COOH-PEG-SH molecules binding on the surface of AuNPs confirming the oxygen signal (O_{1S}), Au signal (Au_{4f}) and carbon signal (C_{1S}). Also, nitrogen signal (N_{1S}) and bromide signal (Br_{3d}) were verified to replace CTAB molecules to PEG-coated gold nanorod and sodium signal (Na_{1S}) was checked for functionalization on the surface of the gold nanosphere (Ulvac PHI, X-tool, X-ray source: Al 1486.6 eV, 24.1 W, 15 kV).

2.5. Zeta potential

Zeta potential measurements indicated ligand binding on the surface of gold nanoparticles through electro-kinetic potential gap between the liquid medium and stationary fluid layer joined to the dispersed particle. After modification of nanoparticles with COOH-PEG-SH molecules, zeta potential decreased to a negative charge by ligand electric potential. (Zeta potential Analyzer, Otsuka Electronics, ELSZ-1000).

3. Results and discussion

3.1. Preparation and featuring of shape-code gold nanoparticles

The platform to detect biomarkers of Alzheimer's disease was fabricated in three different sizes and shapes of gold nanoparticles that are 50 nm gold nanospheres (AuNSs), aspect ratio 1.6 gold nanorods (A.R. 1.6 AuNRs) and A.R. 3.6 AuNRs following Cao's and Murray's way (Ye et al., 2013; Jv et al., 2010). Morphologies of prepared particles were explored through transmission electron microscopy (TEM) images (Fig. S1). Mixed gold nanoparticles solution was dropped on a 400-mesh copper grid and the TEM image that was taken reveals AuNSs and two aspect ratios of AuNRs are well combined (Fig. 2A).

It also is possible to differentiate nanoparticles of distinct sizes and/or shapes in aqueous solution and collect correlated optical spectra of each gold nanoparticle from inhomogeneous nanoparticles solution through LSPR system and UV–vis spectrometry (Truong et al., 2014) (Fig. 2B and C). UV–vis spectra represent max absorbance at specific wavelength allowing for determining the diameter (*d*) and/or concentration of gold nanoparticles from analytical relation (extinction efficiency and *d*) (Haiss et al., 2007). Average diameter of 54 ± 4 nm and concentration of approximately 0.293 nM were collected from Au nanospheres as well gold nanorod particles had grown 58.5 nm × 96 nm and 34.7 nm × 124.8 nm with aspect ratio of 1.64 and 3.59, respectively (Fig. 2B). Shape-dependent light scattering of Au nanoparticles is shown distinctively in Fig. 2C, but wavelengths of LSPR peaks are contiguous with those of maximum absorbance in UV–vis spectra due to specific characters of gold nanoparticles morphologies.

Distinct optical properties enable the shape-code plasmonic biosensor used for ultra-selective detection of various conjugated biomolecules from separate colored spots and plasmon-optical spectra. Gold nanoparticles are recognized with the naked eye in dark field as a bright-colored spot under LSPR system (El-Sayed, 2001). Dark-field images are acquired with experimental apparatus including white-light

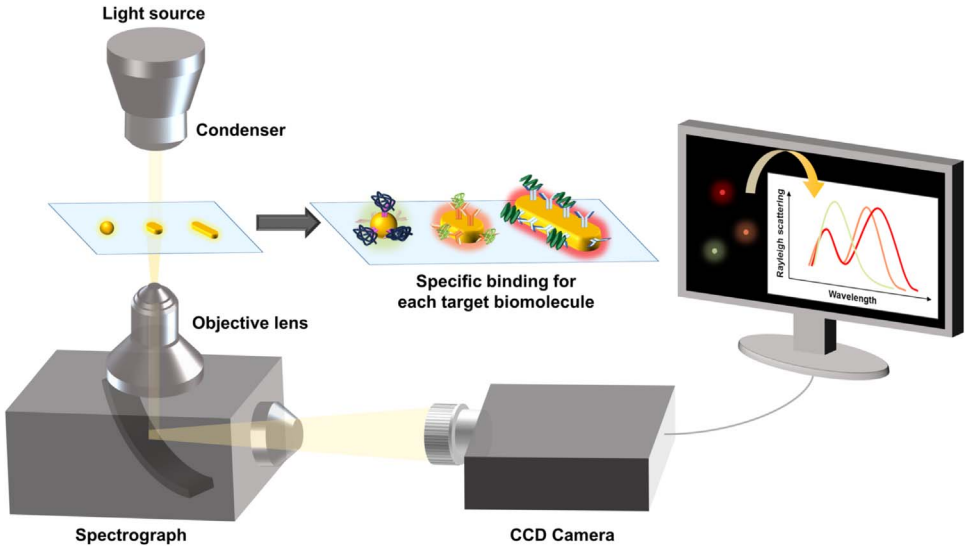

Fig. 1. Schematic illustration of shape-code plasmonic biosensor for multiple Alzheimer's disease biomarkers.

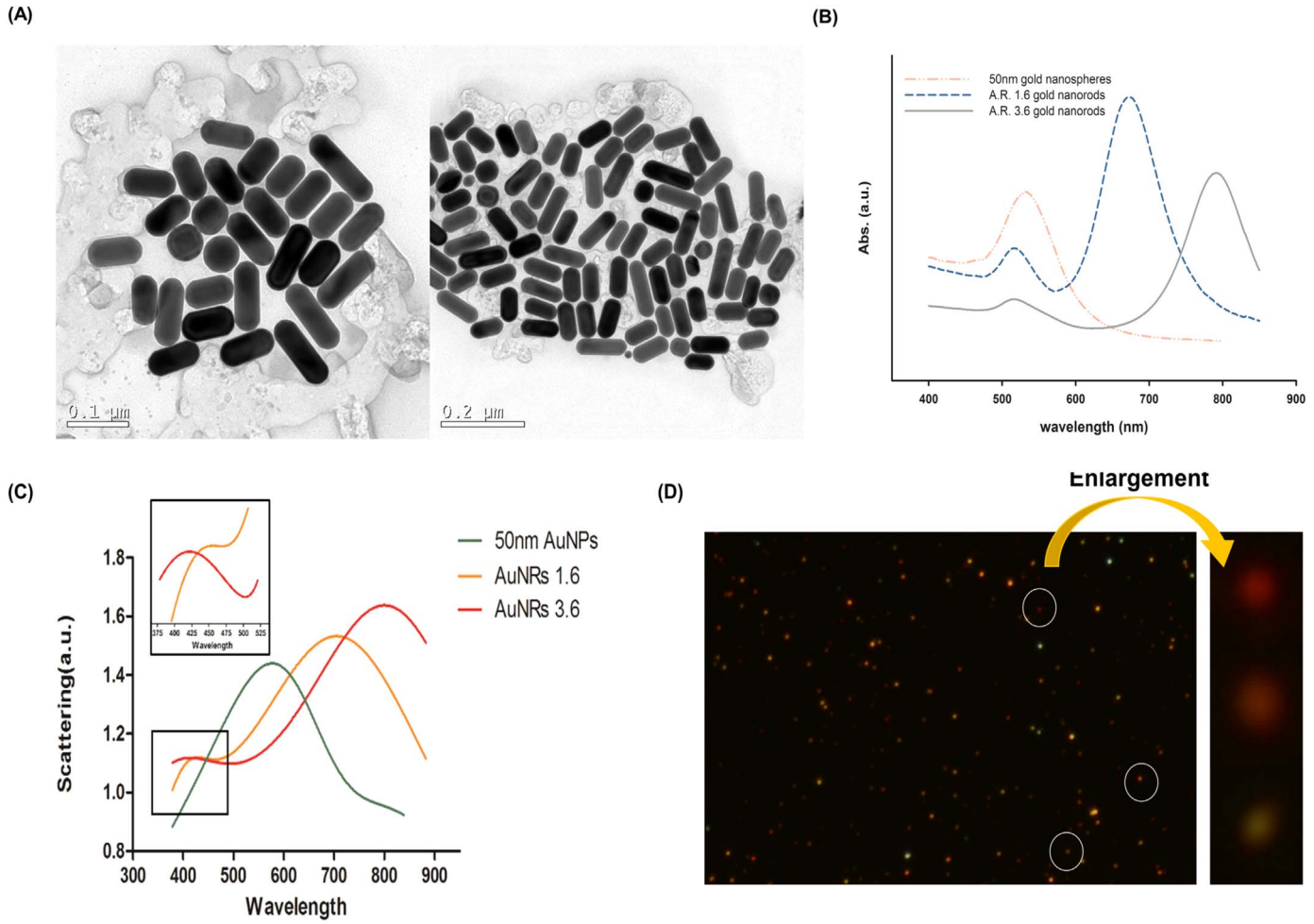

Fig. 2. Plasmon-optical properties of shape-code gold nanoparticles. (A) HR-TEM images of 50 nm AuNSs, aspect ratio 1.6 AuNRs and aspect ratio 3.6 AuNRs (B) UV–vis absorption spectra of shape-code particles (C) representative resonant Rayleigh light scattering spectra of shape-code, fitted to Lorentzian algorithm (D) dark-field images of gold nanoparticles, colored spots depend on shape and size of particles, red for A.R. 3.6 AuNRs, orange for A.R. 1.6 AuNRs and olive green for 50 nm AuNSs at 1000 × magnification. (For interpretation of the references to color in this figure legend, the reader is referred to the web version of this article.)

illuminations enabling one to discriminate light scattering of nanoparticles of different sizes and/or shapes from distinct optical resonances (Wang et al., 2015). For spherical gold nanoparticles of 50 nm diameter, light scattering appears as olive green scattering spots while the shorter AuNRs (A.R. 1.6) and longer AuNRs (A.R. 3.6) appear as orange and red spots under a dark-field microscope, respectively (Fig. 2D). Since AuNPs have a predominant scattering cross-section, strong Rayleigh scattering light of individual particles may be easily recognized under light-scattering dark-field microscopy (Ni et al., 2008; Peng et al., 2015). Furthermore, AuNPs' absorption cross sections are at least five orders larger than those of universal dyes and the light scattering is several orders larger than the light emission from strongly fluorescent dyes (Lee et al., 2005; Jain et al., 2006; Ni et al., 2008). That properties of gold nanoparticles are able to use as sensing applications in area of biology requiring delicately to detect the biomarkers.

In addition, the detection platform can collect quantitative data by the corrected optical spectra shifts of single gold nanoparticles, since gold nanoparticles ultra-sensitively identify binding events of small biological or chemical molecules (< 500 Da) (Kretzschmar et al., 2004; Truong et al., 2014; Song et al., 2016). In the case of proteins, such an assay method may be between one to six times more highly sensitive than a conventional approach and this improved sensitivity provides the opportunity to monitor existing biomarkers at infinitesimal levels in complex samples (Thaxton et al., 2009). Synthetically, shape-code AuNPs may be used as one nanosensor to detect low molecular weight biomarkers separately.

3.2. Construction of plasmonic sensor for multi-detection based on shape-code gold nanoparticles

To stabilize and link with antibody, we functionalized with heterobifunctional polyethylene glycol (COOH-PEG-SH) on the surface of particles. The oxidative addition of the thiol bond to the gold surface initiates gold-thiol reaction followed by reductive elimination of hydrogen (Choi et al., 2012). To estimate completed functionalization to PEG-coated gold nanoparticles (PGNPs) from Bare AuNSs and CTAB-coated AuNRs, X-Ray photoelectron spectroscopy (XPS) spectra and zeta-potential measurement were collected (Table 1, Fig. 3).

Table 1
Relative percentages of XPS elemental composition on coated gold nanoparticles.

Sample	% XPS elemental composition					
	C_{1s}	O_{1s}	Au_{4f}	Na_{1s}	N_{1s}	Br_{3d}
Bare AuNSs	41.35	28.1	21.25	6.65	–	–
PEG-coated AuNSs	53.15	33.7	10.4	2.65	–	–
CTAB-coated A.R. 1.6 AuNRs	91.55	2.4	0.3	–	3.3	2.55
PEG-coated A.R. 1.6 AuNRs	59.2	36.1	1.8	–	0	0
CTAB-coated A.R. 3.6 AuNRs	90.9	1.3	1.45	–	3.85	2.8
PEG-coated A.R. 3.6 AuNRs	61.1	25.4	4.7	–	0	0

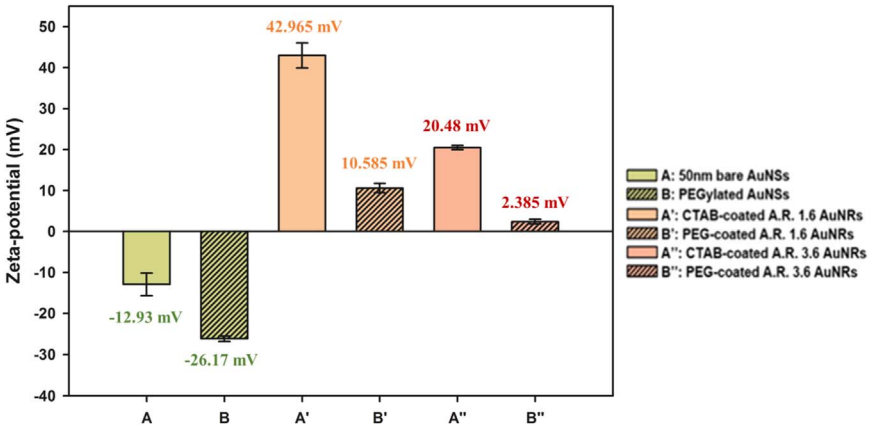

Fig. 3. Zeta potential measurements after PEG surface modification for shape-code plasmonic biosensor synthesis.

XPS is a direct, quantitative analytical method providing detailed chemical structure information on ligand composition of gold nanoparticles, and therefore strong evidence of ligand bonding (Indrasekara et al., 2014). Electromental analyses revealed a significant increase in characteristic oxygen signal (O_{1s}), interpreted as carbon-oxygen bond functionality, due to the emergence of ethylene glycol chain (-CH_2CH_2O-) repeat units on AuNSs and AuNRs surface (Joshi et al., 2013). However, specific XPS peaks of Au_{4f} revealed conflicting results between particles due to PEG molecules coating on surfaces. In the case of gold nanorod, CTAB bilayer was exchanged to a less-dense PEG layer. The exposed surface of AuNRs generated more scattering events and led to an increase Au XPS signal. While the same polymer covered 50 nm bare gold, nanospheres decreased relative percentage of gold elemental composition due to packing of PEG molecules on AuNSs bared surface. The complete displacement of CTAB molecules on AuNRs may be validated by the absence of the bromine signal (Br_{3d}) and the nitrogen signal (N_{1s}) originating from surfactant (Indrasekara et al., 2014).

Zeta-potential measurements indicate that nanoparticles are highly stable and have exact potential difference for polyelectrolytic overcoated gold nanoparticles. For both modifications, surface charges reduced significantly. As shown Fig. 3, surface potential of 50 nm gold nanospheres exhibits -12.93 ± 2.76 mV indicating that citrate molecules are attached on particles electrostatically and became more negative (-26.17 ± 0.64 mV) from dense functionalization by PEG molecules (Ivanov et al., 2009). PEG-coated gold nanorods revealed a rapid shift from positive to approximately neutral level, implying PEG chains bound to nanorods and covered their surface completely even if few cationic surfactants remained on AuNPs surface (A.R. 1.6. AuNRs: $+ 42.965 \pm 3.08$ to $+ 10.585 \pm 1.15$ mV, A.R. 3.6 AuNRs: $+ 20.48 \pm 0.55$ to $+ 2.385 \pm 0.54$ mV) (Niidome et al., 2006). Results are derived from successful surface functionalization of gold nanoparticles with heterofunctional PEG molecules.

After PEGylation of gold nanoparticles, monoclonal antibody (mAb) were bound on the surface of gold nanoparticles through forming chemical bond using with 1-ethyl-3-(3-dimethylaminopropyl) carbodiimide/N-hydroxysuccinimide (EDC-NHS) chemistry between the primary amine (-NH_2) groups and the carboxylic acid group (-COOH) (Choi et al., 2013). Carboxylic acid groups of PEG were converted to reactive NHS-ester groups, active functional groups reacting with residual primary amino groups of antibodies. We determined the conjugation with each antibody and the shape of gold nanoparticles depended on the concentration of target proteins in blood and sensitivity of AuNPs. The antibody capturing the most insufficient marker in blood (e.g. τ protein) was bound on longer gold nanorod (aspect ratio of 3.6), conversely, highest concentration protein (Aβ 1–40) is targeted by mAb-conjugated gold nanospheres. It is the reason for the matching with antibody and shape-code plasmonic biosensor that longer plasmon oscillation time on extended AuNPs occurs more sensitive reaction (Kvasnicka et al., 2008).

UV–vis spectra reveal absorbance shifts after each step for synthesis of the shape-code plasmonic biosensor (Fig. S2). This result was provided by the plasmon resonance phenomenon of AuNPs derived from the changed local refractive index of the particle. Peak shifts to NIR region in the figures indicate that the surface of gold nanoparticles was successfully functionalized by PEG molecules and conjugated with the antibody by amide bonds. The conjugation chemistry for binding on the surface of gold nanoparticles has been well established (Nam et al., 2004), that develop the way to fabricating the shape-code plasmonic biosensor.

The plasmonic biosensor based on shape-code gold nanoparticles were immobilized on the modified glass slide and results in distinct LSPR spectra induced by analyte binding on mAb-conjugated gold measured by dark-field, a spectrograph, and CCD camera. The gold nanoparticle plasmonic biosensor has been suggested as a viable structure to capture the low level of targeting antigens (Nguyen et al., 2015).

3.3. Examination of cross-talk on shape-code plasmonic sensor

Plasma includes over 3700 identified proteins underlying non-specific bindings (Truong et al., 2014). Such cross-reaction of sensors using plasma leads to decrease in target biomarker selectivity and platform's credibility, especially, for multi-analyte assay (Fu et al., 2006). For this reason, in the case of sensors using blood, cross reactivity must always be considered.

In this system, three different antibodies for distinct Alzheimer's disease biomarker were bound on shape-code AuNPs interacting with corresponding target biomarkers to confirm non-cross reactions. LSPR peak shifts of an antigen-specific plasmon biosensors indicate autonomous detection of amyloid- beta (Aβ) 1–40, Aβ 1–42 and τ protein on the immune-50 nm AuNSs, A.R. 1.6 AuNRs and A.R. 3.6 AuNRs, respectively (Fig. 4). Each shape-code particle interacting with corresponding biomarker generated significant LSPR peak shift. Despite 100 nM of each protein were minimum 5000 folds higher than a typical concentration of Aβ 1–40, Aβ 1–42 and τ protein in normal blood, cross-reaction did not occur on shape-code biosensor (Slemmon et al., 2007; Schupf et al., 2008; Zetterberg et al., 2013). The $\Delta\lambda_{max}$ was measured; 1.11 nm and 1.04 nm for Aβ 1–42 and τ protein injected to anti-Aβ 1–40 gold nanospheres respectively, whereas 1.92 nm and 1.95 nm for Aβ 1–40 and τ protein injected to anti-Aβ 1–42 gold nanorods respectively. Aspect ratio 3.6 of gold nanorod biosensor characterized high sensitivity also reveals that the LSPR λ_{max} shift was about 2 nm for binding of non-specific antigens. These results indicate that there was not cross-reactivity between shape-code plasmonic biosensors with negligible nonspecific binding. We confirmed that this 'shape-code' plasmonic biosensor had magnificent selectivity for detection of targeted AD biomarkers in mimicked blood.

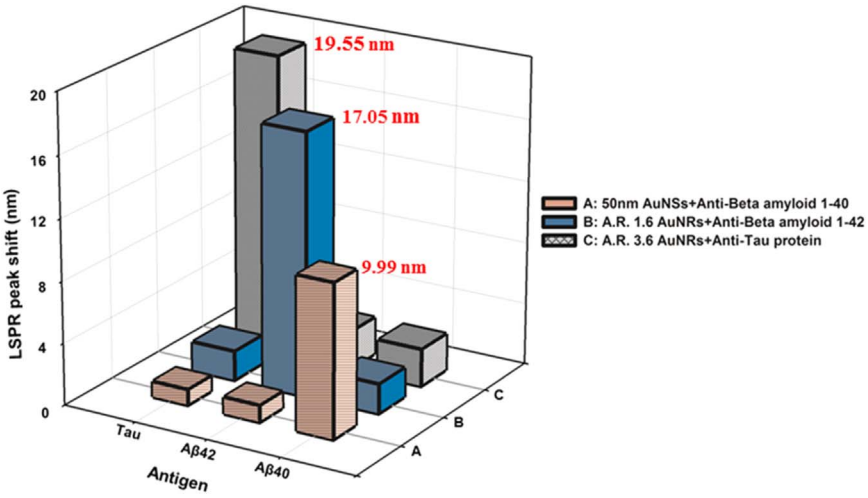

Fig. 4. The LSPR peak shift of shape-code plasmon biosensors for the independent detection of Aβ 1–40, Aβ 1–42 and τ protein.

3.4. Analytical performance of shape-code plasmonic biosensor for multiple detection of Alzheimer's disease biomarker

To verify that this system is optimal system for multiple label-free detection, analytical performance factors, such as sensitivity and specificity of the plasmonic biosensor platform, should be evaluated with various concentration of biomarkers in the mixture (Lee et al., 2015). Under biological conditions of patient-mimicked plasma, multiple biomarkers detection was conducted on a platform consisting of three types immunogold with three Alzheimer's disease biomarkers, Aβ 1–40, Aβ 1–42 and τ protein. LSPR $\Delta\lambda_{max}$ shifts indicated a strong linearity with the concentration logarithm in the range from 1 * 10^1 fM to 1 * 10^8 fM that concentrations are optimized between least twenty times lower and quite higher than levels of biomarkers in AD patient plasma (Fig. 5A). Many coefficients of determination (R^2) were over 0.95 meaning the values of LSPR peak shift are significantly depended on concentrations of samples in mimicked blood. The limit of detection (LOD) values of the biosensor were calculated by this formula: LOD = 3*δ / *slope,* where δ is the standard deviation of blank and *slope* is the slope of calibration curve (Ma et al., 2014). Calculated values were 34.9 fM for Aβ 1–40 with immune 50 nm gold nanosphere, 26 fM for Aβ 1–42 with immune-aspect ratio 1.6 of gold nanorod and 23.6 fM for τ protein with immune-aspect ratio 3.6 of gold nanorod (Fig. 5B). Sensitivity of this multiple-plasmonic sensor platform was satisfactory for applying to practical and clinical assay based on minimal values for another blood-based assay such as double-sandwich ELISA assay which are 4.62 pM for Aβ 1–40, 2.22 pM for Aβ 1–42 and 815.2 fM–1.63 pM for τ protein (Mehta et al., 2000; Randall et al., 2013; Schupf et al., 2008). The level of the three AD core proteins in blood were approximately measured about 51.8 pM, 2.7 pM and 239.13 fM, in order, Aβ 1–40, Aβ 1–42 and τ protein, in an Alzheimer's disease patient, respectively, after four to five years follow-up studies (Van Oijen et al., 2006; Zetterberg et al., 2013; Randall et al., 2013). Results support our proposed system enabling validity of clinical evidence with high accuracy in complex human biological fluids. Additionally, we validated that this plasmonic biosensor is a simple LSPR platform for detection of multiple targeted biomolecules and quantification of various proteins by analyzing changed value of LSPR peak shift. This multiplex LSPR biosensor is a promising candidate for diagnostic platform of multiple analytes with high sensitivity and select-ability in rapid and simple format.

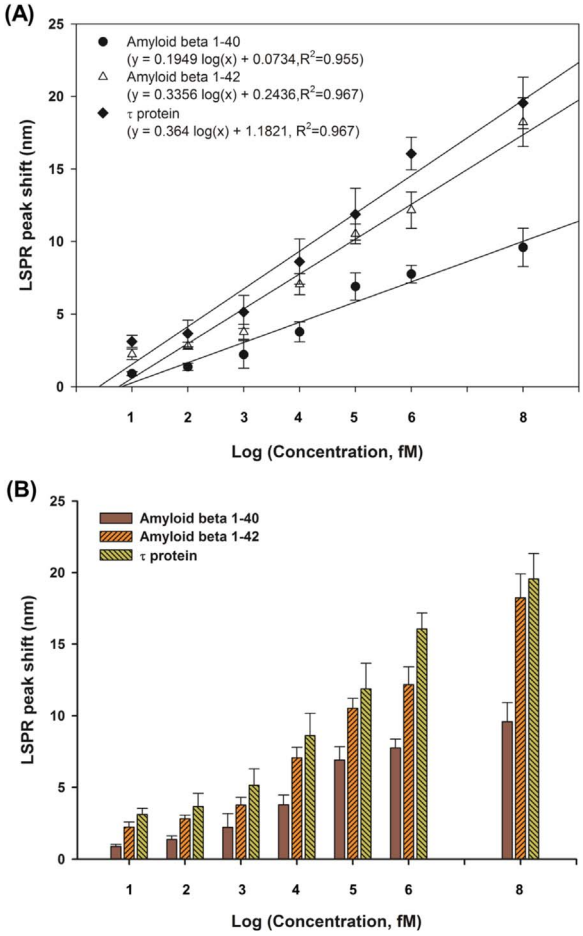

Fig. 5. (A) Linear regression of the calibration curve describing the relationship between the LSPR wavelengths peak shifts and Aβ 1–40, Aβ 1–42 and τ protein concentrations (B) detection of Aβ 1–40, Aβ 1–42 and τ protein at concentrations ranging from 10 fM to 10^8 fM using mimic plasma.

4. Conclusion

We demonstrated that the shape-code plasmonic biosensor enabled the selective detection of Alzheimer's disease core proteins on a platform. This plasmonic sensor consisted of three different shapes and sized gold nanoparticles based on the distinct plasmonic characteristics of single nanoparticles with an ultra-selective and colorimetric detection system for multi-analytes. By simply measuring LSPR $\Delta\lambda_{max}$ shift, we can detect AD core three proteins and quantify the amount of those biomarkers used to investigate AD in a one-step multiple detection system directly. This plasmonic platform for multiplex detection of AD

biomarkers is capable of easy analyses with optical-colorimetric properties, reduction in result error range and a comparable reduction of sample volumes. Thus, our proposed plasmonic biosensor can validate clinical evidence with high accuracy, effectively, and be a promising candidate for diagnostic platform of multiple analytes with high sensitivity and select-ability in rapid and simple format.

Acknowledgment

This study was supported by the National Research Foundation of Korea (NRF) grants (Grant No. NRF-2016R1A2A1A05005465/2010-0027955) and grants (2014M1A8A1049278) from the Korea CCS R & D Center (Korea CCS 2020 Project) grant funded by the Korea government (Ministry of Science and ICT) in 2017.

Appendix A. Supplementary material

Supplementary data associated with this article can be found in the online version at http://dx.doi.org/10.1016/j.bios.2017.10.018.

References

Abdi, F., Quinn, J.F., Jankovic, J., McIntosh, M., Leverenz, J.M., Peskind, E., Nixon, R., Nutt, J., Chung, K., Zabetian, C., Samii, A., Lin, M., Hattan, S., Pan, C., Wang, Y., Jin, J., Zhu, D., Jane Li, G., Liu, Y., Waichunas, D., Thomas, J., 2006. J. Alzheimers Dis. 9, 293–348.
Anker, J.N., Hall, W.P., Lyandres, O., Shah, N.C., Zhao, J., Van Duyne, R.P., 2008. Nat. Mater. 7, 442–453.
Butterfield, D.A., Boyd-Kimball, D., Castegna, A., 2003. J. Neurochem. 86, 1313–1327.
Carrette, O., Demalte, I., Scherl, A., Yalkinoglu, O., Corthal, G., Burkhard, P., Hochstrasser, D.F., Sanchez, J.C., 2003. Proteomics 3, 1486–1494.
Choi, J., Yang, J., Bang, D., Park, J., Suh, J.-S., Huh, Y.-M., Haam, S., 2012. Small 8, 746–753.
Choi, J., Park, Y., Choi, E.B., Kim, H.-O., Kim, D.J., Hong, Y., Ryu, S.-H., Lee, J.H., Suh, J.-S., Yang, J., Huh, Y.-M., Haam, S., 2013. J. Biomed. Opt. 19, 051203.
Citron, M., Teplow, D.B., Selkoe, D.J., 1995. Neuron 14, 661–670.
El-Sayed, M.A., 2001. Acc. Chem. Res. 34, 257–264.
Frank, R.A., Galasko, D., Hampel, H., Hardy, J., De Leon, M.J., Mehta, P.D., Rosers, J., Siemers, E., Trojanowski, J.Q., 2003. Neurobiol. Aging 24, 521–536.
Fu, Z.F., Liu, H., Ju, H.X., 2006. Anal. Chem. 78, 6999–7005.
Gish, D.A., Nsiah, F., McDermott, M.T., Brett, M.J., 2007. Anal. Chem. 79, 4228–4232.
Gupta, V.B., Sundaram, R., Martins, R.N., 2013. Alzheimers Res. Ther. 5, 31–36.
Haiss, W., Thanh, N.T.K., Aveyard, J., Fernig, D.G., 2007. Anal. Chem. 79, 4215–4221.
Hall, W.P., Ngatia, S.N., Van Duyne, R.P., 2011. J. Phys. Chem. C 115, 1410–1414.
Hye, A., Lynham, S., Thambisetty, M., Causevic, M., Campbell, J., Byers, H.L., Hooper, C., Rijsdijk, F., Tabrizi, S.J., Banner, S., Shaw, C.E., Foy, C., Poppe, M., Archer, N., Hamilton, G., Powell, J., Brown, R.G., Sham, P., Ward, M., Lovestone, S., 2006. Brain 129, 3042–3050.
Indrasekara, A.S.D.S., Wadams, R.C., Fabris, L., 2014. Part. Part. Syst. Charact. 31, 819–838.
Ivanov, M.R., Bednar, H.R., Haes, A.J., 2009. ACS Nano 3, 386–394.
Jain, P.K., Lee, K.S., El-Sayed, M.A., 2006. J. Phys. Chem. B 110, 7238–7248.
Joshi, P.P., Yoon, S.J., Hardin, W.G., Emelianov, S., Sokolov, K.V., 2013. Bioconjug. Chem. 24, 878–888.
Jv, Y., Li, B., Cao, R., 2010. Chem. Commun. 46, 8017–8019.
Kanekiyo, T., Xu, H., Bu, G., 2014. Neuron 81, 740–754.
Kang, J.-H., Vanderstichele, H., Trojanowski, J.Q., Shaw, L.M., 2012. Methods 56, 484–493.
Kretzschmar, A.K., Dinger, M.G., Henze, C., Brocke–Heidrich, K., Horn, F., 2004. Biochem. J. 377, 289–297.
Kvasnicka, P., Homola, J., 2008. Biointerphases 8, 4–11.
Lee, J.U., Nguyen, A.H., Sim, S.J., 2015. Biosens. Bioelectron. 74, 341–346.
Lee, K.-S., El-Sayed, M.A., 2005. J. Phys. Chem. B 109, 20331–20338.
Liao, Y.-H., Chang, Y.-J., Yoshiike, Y., Chang, Y.-C., Chen, Y.-R., 2012. Small 8, 3631–3639.
Link, S., El-Sayed, M.A., 2000. Int. Rev. Phys. Chem. 19, 409–453.
Liu, C.-C., Kanekiyo, T., Xu, H., Bu, G., 2013. Nat. Rev. Neurol. 9, 106–118.
Ma, W., Yin, H., Xu, L., Wu, X., Kuang, H., Wang, L., Xu, C., 2014. Chem. Commun. 50, 9737–9740.
Martin, L., Latypova, X., Terro, F., 2011. Neurochem. Int. 58, 458–471.
McFarland, A.D., Duyne, R.P.V., 2003. Nano Lett. 3, 1057–1062.
Mehta, P.D., Pirttilä, T., Mehta, S.P., Sersen, E.A., Aisen, P.S., Wisniewski, H.M., 2000. Arch. Neurol. 57, 100–105.
Nam, J.-M., Stoeva, S.I., Mirkin, C.A., 2004. J. Am. Chem. Soc. 126, 5932–5933.
Nguyen, A.H., Sim, S.J., 2015. Biosens. Bioelectron. 67, 443–449.
Ni, W., Kou, X., Yang, Z., Wang, J., 2008. ACS Nano 2, 677–686.
Niidome, T., Yamagata, M., Okamoto, Y., Akiyama, Y., Takahashi, H., Kawato, T., Katayama, Y., Niidome, Y., 2006. J. Control. Release 114, 343–347.
Peng, Y., Xiong, B., Peng, L., Li, H., He, Y., Yeung, E.S., 2015. Anal. Chem. 87, 200–215.
Randall, J., Mörtberg, E., Provuncher, G.K., Fournier, D.R., Duffy, D.C., Rubertsson, S., Blennow, K., Zetterberg, H., Wilson, D.H., 2013. Resuscitation 84, 351–356.
Rosi, N.L., Mirkin, C.A., 2005. Chem. Rev. 105, 1547–1562.
Schneider, P., Hampel, H., Buerger, K., 2009. CNS Neurosci. Ther. 15, 358–374.
Schupf, N., Tang, M.X., Fukuyama, H., Manly, J., Andrews, H., Mehta, P., Ravetch, J., Mayeux, R., 2008. Proc. Natl. Acad. Sci. USA 105, 14052–14057.
Shaw, L.M., Vanderstichele, H., Knapik-Czajka, M., Clark, C.M., Aisen, P.S., Petersen, R.C., Blennow, K., Soares, H., Simon, A., Lewczuk, P., Dean, R., Siemers, E., Potter, W., Lee, V.M., Trojanowski, J.Q., 2009. Ann. Neurol. 65, 403–413.
Slemmon, J.R., Painter, C.L., Nadanaciva, S., Catana, F., Cook, A., Motter, R., Seubert, P., 2007. J. Chromatogr. B 846, 24–31.
Song, S., Nguyen, A.H., Lee, J.U., Cha, M., Sim, S.J., 2016. Analyst 141, 2493–2501.
Stoeva, S.I., Lee, J.-S., Smith, J.E., Rosen, S.T., Mirkin, C.A., 2006. J. Am. Chem. Soc. 128, 8378–8379.
Thaxton, C.S., Elghanian, R., Thomas, A.D., Stoeva, S.I., Lee, J.-S., Smith, N.D., Schaeffer, A.J., Klocker, H., Horninger, W., Bartsch, G., Mirkin, C.A., 2009. Proc. Natl. Acad. Sci. USA 106, 18437–18442.
Truong, P.L., Kim, B.W., Sim, S.J., 2012. Lab Chip 12, 1102–1109.
Truong, P.L., Ma, X., Sim, S.J., 2014. Nanoscale 6, 2307–2315.
Van Oijen, M., Hofman, A., Soares, H.D., Koudstaal, P.J., Breteler, M.M., 2006. Lancet Neurol. 5, 655–660.
Wang, Y., Zou, H.Y., Huang, C.Z., 2015. Nanoscale 7, 15209–15213.
Ye, X., Zheng, C., Chen, J., Gao, Y., Murray, C.B., 2013. Nano Lett. 13, 765–771.
Zetterberg, H., Wilson, D., Andreasson, U., Minthon, L., Blennow, K., Randall, J., Hansson, O., 2013. Alzheimers Res. Ther. 5, 9.